Applied Catalysis B: Environmental 185 (2016) 174–180

Contents lists available at ScienceDirect

Applied Catalysis B: Environmental

journal homepage: www.elsevier.com/locate/apcatb

Photo-redox reactions of indole and ferric iron in water

Sonja Milić Komić[a], Jelena Bogdanović Pristov[a], Ana Popović-Bijelić[b], Joanna Zakrzewska[c], Marina Stanić[a], Aleksandar Kalauzi[a], Ivan Spasojević[a,*]

[a] Department of Life Sciences, Institute for Multidisciplinary Research, University of Belgrade, 11030 Belgrade, Serbia
[b] EPR Laboratory, Faculty of Physical Chemistry, University of Belgrade, 11158 Belgrade, Serbia
[c] NMR Laboratory, Institute of General and Physical Chemistry, 11000 Belgrade, Serbia

ARTICLE INFO

Article history:
Received 10 August 2015
Received in revised form 2 December 2015
Accepted 11 December 2015
Available online 12 December 2015

Keywords:
Indole
Iron
UV
Ligand
Free radical

ABSTRACT

Iron–organic interactions are involved in a variety of environmental phenomena, including photo-redox reactions, iron cycling and bioavailability, as well as contaminant fate. In this study we examined UV-induced redox reactions of iron and indole in water. The presence of one indole in the irradiated system resulted in the presence of eight reduced ferric ions, not counting direct photolysis of Fe^{3+} complexes with OH^-, which gives Fe^{2+} and hydroxyl radical ($HO^\bullet$) as products. The main mechanisms that contribute to indole-related Fe^{3+} reduction *i.e.* Fe^{2+} accumulation are: (i) $HO^\bullet$ scavenging, which prevents oxidation of Fe^{2+} by $HO^\bullet$; (ii) oxidation of indole and its derivatives by excited ferric iron; (iii) reduction of ferric iron by excited indole (not present under UV-A). Hydrated electrons released by UV-B-excited indole play only a minor role in the reduction of iron. Indole-derived radicals emerged as byproducts of indole/iron photochemistry. ^{1}H NMR and low-T EPR spectroscopy showed that indole forms a weak low-symmetry complex with Fe^{3+}. The strongest interactions between iron and π-cloud in the indole ring are at positions 2, 3, and 7. The formation of complex promotes electron transfer from excited indole to Fe^{3+}. Our findings are important for understanding the catalysis of photo-reduction of iron by heterocyclic aromatic pollutants, and for the development of protocols for indole processing in wastewaters.

1. Introduction

Photo-redox reactions of iron in surface waters are involved in: (i) regulation of iron cycling and bioavailability; (ii) production of different reactive species; and (iii) oxidation of organic pollutants and natural organic matter. They act as environmental sinks for different contaminants and have been applied as advanced oxidation processes in wastewater treatment [1–3]. Photo-reduction of Fe^{3+} to Fe^{2+} involves ligand-to-iron electron transfer. The main route for UV-induced iron reduction in aerobic water systems (*e.g.* streams, collected rain, bog water, some lakes, estuaries) is photolysis of complexes of ferric iron and hydroxyl ion(s)—$Fe(OH)^{2+}$ and $Fe(OH)_2{}^+$ [2]. The rate of the Fe^{3+} photo-reduction does not change significantly within 3–5 pH range [4], which is characteristic for these waters [3,5]. Ferrous iron is significantly more soluble and available to living systems compared to Fe^{3+}, and it participates in other redox processes (*e.g.* Fenton reaction) acting as an electron shuttle [5]. Hydroxyl radical ($HO^\bullet$) is a by-product of photolysis of $Fe(OH)^{2+}$ and $Fe(OH)_2{}^+$. Iron can also form coordination bonds and different types of interactions with organic ligands. Ligands are involved in all the aspects of environmental (bio)chemistry of iron, affecting reduction potential, redox chemistry and solubility of iron [6,7]. Ferric iron can be reduced by the excited ligands or by organic radicals and other products that emerge in photo-reactions. Alternatively, excited ferric iron might oxidize organic ligands [5]. When it comes to iron reduction, aromatic compounds are the most important component of organic matter [8]. This is clearly demonstrated by the fact that aromaticity is the only parameter that shows significant positive correlation with iron-reducing capacity of organics in aquatic systems [5]. It has been estimated that the rate of interactions of environmental UV irradiation with organic molecules and iron in water is rather high, representing a 'motor' for transformation of chemicals [1]. UV-B (280–320 nM) and UV-A (320–400 nm) irradiance varies significantly with latitude and altitude, and may be as high as 5 and 70 $J\,m^{-2}\,s^{-1}$ at sea level [9]. In autumn, at 50th parallel north, UV-B and UV-A are around 1 and 25 $J\,m^{-2}\,s^{-1}$, respectively [10].

* Corresponding author at: Institute for Multidisciplinary Research, Kneza Višeslava 1, 11030 Belgrade, Serbia. Fax: +381 11 3055289.
E-mail addresses: ivan@imsi.rs, redoxsci@gmail.com (I. Spasojević).

http://dx.doi.org/10.1016/j.apcatb.2015.12.018
0926-3373/

Indole is *N*-heterocyclic aromatic pollutant found in coking, livestock farms, chemical (pesticide, pharmaceutical) industry, and municipal wastewaters [11–13]. It is also present in non-polluted natural aquatic systems as a product of decomposition of proteins (tryptophan). Indole shows high water solubility (~2 g/L) due to hydrogen bonding with water molecules [14]. Indole represents an electron-rich chromophore, meaning that: (i) it can act as a reductant and it represents a good target for oxidizing agents; (ii) it can be excited; and (iii) it can interact with iron [15]. It has been proposed that excited indole in water undergoes photoionization to produce hydrated electron (e_{aq}^-) and indole radical cation ($Ind^{\bullet+}$) [16,17]. It is noteworthy that reactions with $HO^\bullet$ appear to be an efficient way for indole degradation [18]. This radical is highly reactive and has been widely applied in the treatment of organic pollutants [19].

Using UV-B to simultaneously excite iron and indole and UV-A to excite only iron, we examined the ability of indole to catalyze the reduction of ferric iron and to sustain ferrous iron accumulation. ^{1}H NMR and low-T EPR were employed to investigate the formation of iron–indole complexes.

2. Experimental

2.1. Reagents

All chemicals were of analytical grade and purchased from commercial suppliers: indole and $FeCl_2$ (Merck, Darmstadt, Germany), $FeCl_3$, NaCl, and D_2O (Sigma–Aldrich, St. Louis, MO, USA), H_2O_2 (Carlo Erba Reagents, Milano, Italy), DEPMPO (5-diethoxyphosphoryl-5-methyl-1-pyrroline-*N*-oxide; Enzo Life Sciences International, Plymouth Meeting, PA, USA), DMPO (5,5-dimethyl-1-pyrroline-*N*-oxide; Abcam, Cambridge, UK). All experiments were performed using bidistilled deionized ultrapure (18 MΩ) water. Stock solutions of indole (5 mM) were prepared in water with heating. Indole kept on ice and in the dark was stabile (no changes in the UV/vis spectrum were observed) during the period in which the experiments were conducted (up to 8 h).

2.2. UV irradiation

Samples were prepared in 1 mL of water, placed in a quartz cuvette (1 × 1 × 5 cm), and immediately exposed to UV for 10 min using a lamp with filter for visible light (Carl Roth GmbH, Karlsruhe, Germany; H469.1) and UV tubes (Sankyo Denki, Tokyo, Japan). UV-B and UV-A lamps had maximal emissions at 312 nm and 352 nm, respectively (Fig. S1). Irradiation was conducted in a temperature-regulated chamber (20 °C). Irradiance was 6 J m^{-2} s^{-1} (3 J m^{-2} s^{-1} in experiments with NaCl) for UV-B and 3 J m^{-2} s^{-1} for UV-A.

2.3. UV/vis spectroscopy

UV/vis spectra were recorded using 2501 PC Shimadzu spectrophotometer (Kyoto, Japan) at 20 °C. Measurements were conducted immediately after sample preparation (for non-irradiated systems), or 30 s after the end of irradiation. Scan time was 50 s.

2.4. EPR spectroscopy

Varian E104-A EPR spectrometer operating at X-band (9.51 GHz) with EW software (Scientific Software, Bloomington, IL, USA) was employed for EPR spin-trapping experiments. Measurements were performed at room temperature with the following settings: microwave power, 20 mW; scan time, 2 min; modulation amplitude, 2 G; modulation frequency, 100 kHz. Production of free radicals was examined in the following systems exposed to irradiation: (i) $FeCl_3$ (100 μM) in the absence or in the presence of indole (200 μM), with spin-trap DEPMPO (4 mM); (ii) H_2O_2 (250 μM) with or without indole (200 μM) and with DEPMPO (4 mM); (iii) indole (5 mM) with spin-trap DMPO (40 mM). Spin-traps were supplemented prior to irradiation. Samples were drawn into 10 cm-long gas-permeable Teflon tubes (internal diameter, 0.6 mm; wall thickness, 0.025 mm; Zeus industries, Raritan, NJ, USA), to maintain constant O_2 level, and placed in quartz capillaries. Signal identification and intensity (I) and amplitude quantification were performed *via* simulations in WINEPR SimFonia software (Bruker Analytische Messtechnik GmbH, Darmstadt, Germany). Simulation parameters for DEPMPO/OH adduct were: a_N = 14 G, a_H = 13.2 G, a_H^γ = 0.3 G (3H), and a_P = 47.3 G. Simulation parameters for DMPO adducts: DMPO/OH: a_N = 14.9 G, a_H = 14.8 G; DMPO/H: a_N = 16.6 G, a_H = 22.5 G; DMPO/D: a_N = 16.6 G, $a_{H\beta}$ = 22.5 G, $a_{D\beta}$ = 3.4 G; DMPO/OD: same as for DMPO/OH [20,21]. Anti-$HO^\bullet$ activity of indole was determined using the formula: $(I_{control} - I_{indole})/I_{control}$.

Low-T EPR spectra of non-irradiated water solutions of Fe^{3+}, Fe^{3+}/indole, and Fe^{3+}/indole/NaCl (0.2/1/1 mM) were recorded at 20 K on a Bruker Elexsys-II EPR spectrometer with an Oxford Instruments ESR900 helium cryostat, operating at X-band (9.4 GHz) under the following conditions: microwave power, 3.17 mW; scan time, 80 s; modulation amplitude, 3 G; modulation frequency, 100 kHz; number of accumulations, 4. All spectra were baseline corrected. EPR spectra of indole radicals were recorded at 108 K on a Bruker Elexsys-II EPR spectrometer with Bruker N_2 Temperature Controller ER4131VT, using the same settings, except for scan time (20 s). Samples were placed in quartz EPR tubes immediately after preparation or irradiation, and quickly frozen in cold isopentane.

2.5. Oximetry

[O_2] was determined using a Clark type oxygen electrode (Hansatech Instruments Ltd., King's Lynn, UK) operating with Logger Pro 3 software (Vernier, Beaverton, OR, USA). Experiments were performed in closed-chamber setup (with quartz top), in 5 mL of water with indole (0.2 or 1 mM) and/or $FeCl_3$ (100 μM). All systems were recorded for 5 min before the irradiation to establish the stability of baseline and zero rate of O_2 change. Samples were irradiated inside the chamber for 10 min with UV-B or UV-A, and [O_2] was continually monitored for additional 5 min. Temperature was maintained at 20 °C.

2.6. ^{1}H NMR spectroscopy

^{1}H NMR spectra of non-irradiated indole (200 μM) in the absence or in the presence of $FeCl_3$ (100 μM), $FeCl_2$ (100 μM), and/or NaCl (1 mM) were recorded on Bruker Avance III 500 spectrometer with TopSpin v3.2 interface, using 5 mm BBO probe-head, at 298 K. All samples (and solutions) were prepared in D_2O and placed in 5 mm quartz tubes. Residual HDO signal at 4.7 ppm was used as chemical shift reference. Spectra were analyzed in MestReC v4.5.6 (Mestrelab Research, Santiago de Compostela, Spain).

2.7. Statistical analysis

All experiments were performed in triplicate on separate experimental days. Statistical analysis was performed in STATISTICA 8.0 (StatSoft Inc., Tulsa, OK, USA) using nonparametric 2-tailed Mann–Whitney test ($P < 0.05$) and optimal curve fitting protocols. The goodness of fits was evaluated by R^2 (the adjusted *r*-square value) which accounts for the degrees of freedom.

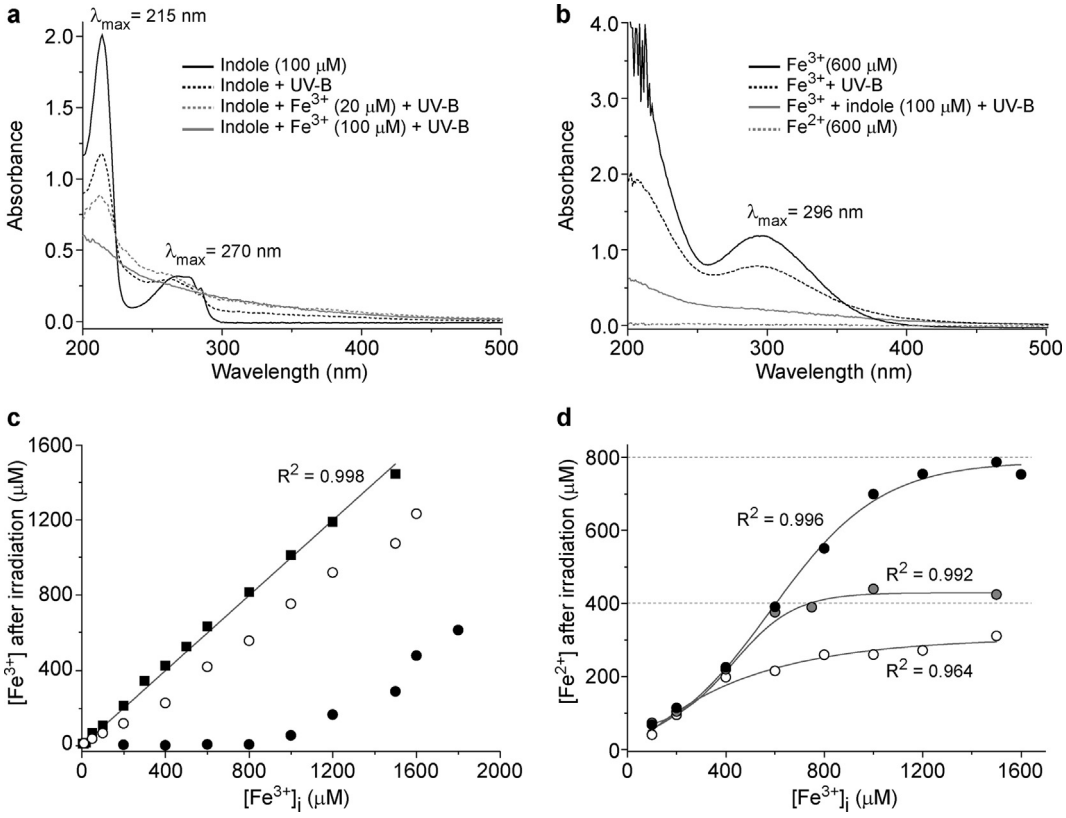

Fig. 1. Indole/Fe^{3+} system exposed to UV-B. (a) UV/vis spectra of indole with or without exposure to UV in the absence or in the presence of Fe^{3+}. (b) UV/vis spectra of ferric iron before and after UV irradiation in the absence or in the presence of indole. (c) The concentration of Fe^{3+}. Squares—untreated samples (controls); gray line—calibration curve (linear fit between real and calculated iron concentrations). Open circles—samples exposed to UV in the absence of indole; Filled circles—samples exposed to UV in the presence of indole (100 μM); (d) The amount of iron reduced by: UV (open cycles), UV + 100 μM indole (filled black cycles), or UV + 50 μM indole (filled gray cycles). Gray lines—sigmoidal fit. R^2 represents a measure of the goodness of fit.

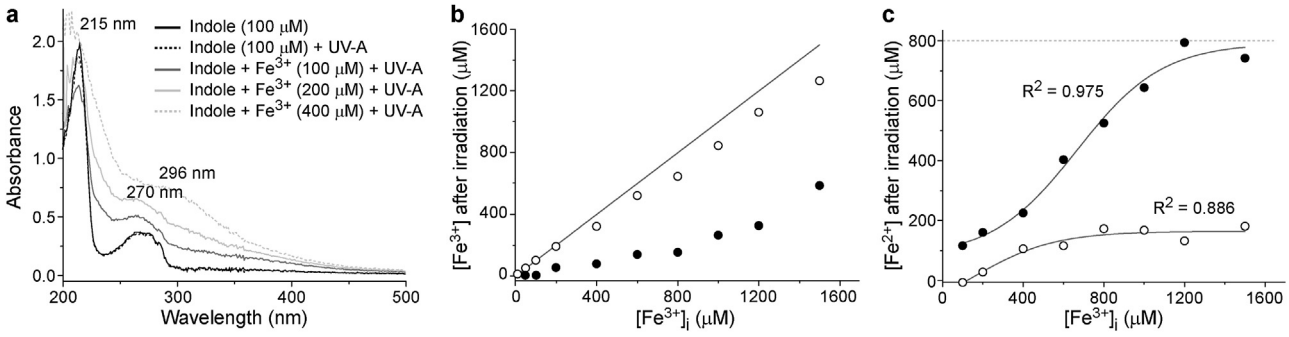

Fig. 2. Indole/Fe^{3+} system exposed to UV-A. (a) UV/vis spectra of indole with or without exposure to UV in the absence or in the presence of Fe^{3+}. (b) The concentration of ferric iron in the system after irradiation. Gray line—calibration curve. Open circles—samples exposed to UV in the absence of indole; Filled circles—samples exposed to UV in the presence of indole (100 μM). (c) The amount of iron reduced by: UV (open cycles) or UV + 100 μM indole (filled cycles). Gray line—sigmoidal fit (R^2 represents a measure of the goodness of fit).

3. Results and discussion

3.1. The reduction of iron by indole under UV irradiation

Fig. 1a shows characteristic UV/vis spectrum of indole. Following UV-B irradiation, the intensity of bands at 215 nm and ~270 nm (assigned to singlet π–π^* transition) was decreased. This can be attributed to photoionization-related reactions. UV-B-induced changes were promoted by ferric iron. Indole bands were diminished in the presence of 100 μM $[Fe^{3+}]_i$ (initial concentration), and only an exponentially decreasing absorbance curve could be observed (Fig. 1a). A similar curve was obtained for systems with $[Fe^{3+}]_i$ in the 200–800 μM range (example in Fig. 1b; all spectra in Fig. S2). Fig. 1b shows the spectrum of ferric iron in water. It appears to represent a sum of spectra of $Fe(OH)^{2+}$ and $Fe(OH)_2{}^+$ that share a common λ_{max} at ~300 nm [22,23]. UV-B irradiation caused Fe^{3+} reduction both in the presence (Fig. S2) and in the absence of indole (Fig. S3). Fe^{2+} shows a negligible absorbance in the concentration range applied here (Fig. 1b). In the 10–800 μM range, no Fe^{3+}-related bands could be observed following irradiation with indole (100 μM). They finally emerged in the irradiated system with 1 mM $[Fe^{3+}]_i$ (Fig. S2). Fig. 1c shows concentrations of Fe^{3+} following the irradiation with or without the indole. The concentrations were calculated based on the absorbance at 296 nm that was corrected for the uniform absorbance of UV-B-irradiated indole/Fe^{3+} systems with $[Fe^{3+}]_i \leq 800$ μM, and then subtracted

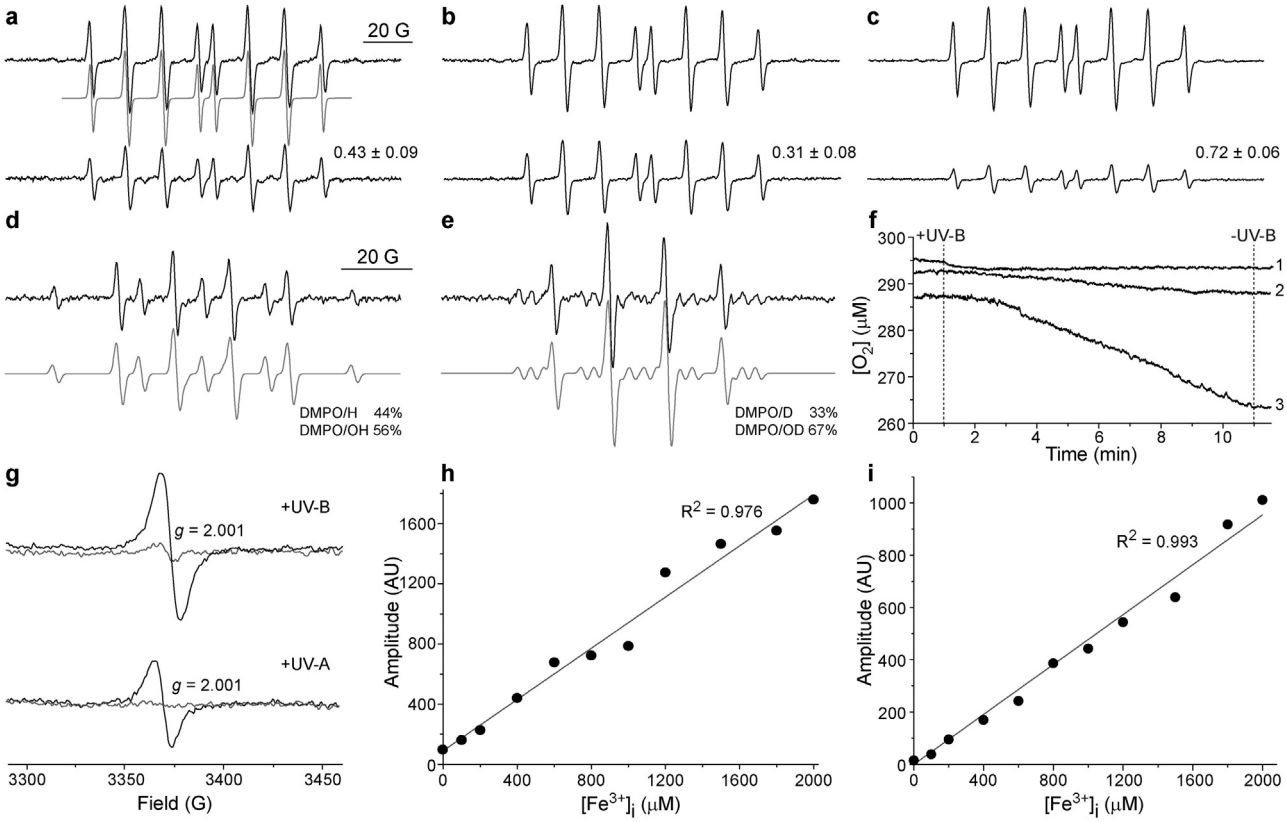

Fig. 3. Formation of free radicals in Fe^{3+}/indole systems exposed to UV. (a) EPR spectra of DEPMPO/OH adduct (gray—spectral simulation) in UV-B-irradiated Fe^{3+} (100 μM) system without (top) or with indole (200 μM; bottom). Relative decrease of DEPMPO/OH signal intensity in the presence of indole is presented as the mean ± SD. (b) EPR spectra of DEPMPO/OH in UV-A-irradiated Fe^{3+} (100 μM) system without (top) or with indole (200 μM; bottom). (c) EPR spectra of DEPMPO/OH in H_2O_2 (250 μM) photolysis system without (top) or with indole (200 μM; bottom). H_2O_2 concentration was tuned to achieve similar yield of DEPMPO/OH as in previous two control systems. (d) EPR spectrum of DMPO adducts following UV-B irradiation of indole (5 mM) in H_2O (e) EPR spectrum of DMPO adducts following UV-B irradiation of indole (5 mM) in D_2O (pH was ~5). Gray—spectral simulations (contribution of each adduct is presented in %). (f) [O_2] in different systems exposed to UV-B. Trace 1—pure water; 2—indole (200 μM); 3—Indole (1000 μM). (g) 108 K EPR spectra of indole (1 mM) exposed to UV in the absence (gray) or in the presence of 1 mM Fe^{3+} (black line). (h) Changes of the amplitude of signal of indole radical(s) with increasing $[Fe^{3+}]_i$ in UV-B-irradiated systems. (i) Change of the amplitude of signal of indole radical(s) with increasing $[Fe^{3+}]_i$ in UV-A-irradiated systems. Gray—linear fit (R^2 represents a measure of the goodness of fit).

from absorbance in indole-free UV-B-irradiated systems with the same $[Fe^{3+}]_i$ to exclude direct effects of UV-B on ferric iron. It is important to note that the limit for $[Fe^{3+}]_i$ (1500 μM) was imposed by absorbance saturation in non-irradiated indole-free systems. Capacities of UV-B and indole to reduce Fe^{3+} are also presented as [Fe^{2+}] following irradiation (Fig. 1d). It can be observed from the sigmoidal fit that 100 μM indole can reduce 800 μM of Fe^{3+}. The same experiments were conducted using 50 μM indole which reduced a maximum of 400 μM Fe^{3+}.

Next we applied UV-A irradiation to discriminate the effects of iron and indole excitation. As expected, the irradiation of iron-free system did not result in any changes in the UV/vis spectrum of indole (Fig. 2a). However, in the presence of iron, changes took place. Indole band with λ_{max} = 270 nm was diminished at 400 μM $[Fe^{3+}]_i$. Ferric iron band (λ_{max} = 296 nm) emerged at $[Fe^{3+}]_i$ = 200 μM, and continued to rise with increasing $[Fe^{3+}]_i$ (Fig. 2b; Fig. S2). The ability of UV-A and indole to reduce Fe^{3+} was evaluated using a similar approach to that used for UV-B. The absorption at 296 nm for irradiated system with 200 μM $[Fe^{3+}]_i$ and indole, was used for correction. It can be observed that the presence of 1 indole resulted in 8 reduced Fe^{3+} ions (Fig. 2c). Clearly, excitation of indole is not obligatory for Fe^{3+} reduction. During the irradiation, pH of all systems remained in the 4.5–5 range (examples in Fig. S4). It is important to note that spectra of ferric iron did not show absorbance at wavelengths >400 nm (Fig. S3). A long wavelength 'tail' could be observed only in the absorption spectra of treated indole, and probably originates from the products of indole decomposition. The established total photochemical reducing capacity of 8 moles of electrons/mole of indole appears to be in good agreement with aromatic properties of indole. According to Hückel's rule ($4n + 2$), indole ring is a ten π -electron system, which consists of eight electrons from C atoms and one lone electron pair from N atom [24].

3.2. Mechanisms of indole-mediated reduction of iron under UV

Mechanisms of Fe^{3+} reduction by indole under UV-B irradiation might involve: (i) scavenging of HO• by indole and its products to prevent reverse reaction, *i.e.* oxidation of Fe^{2+} by HO• ($k = 2.3 \times 10^8\ M^{-1}\ s^{-1}$ [25]); (ii) reduction by e_{aq}^- ($k = 6 \times 10^{10}\ M^{-1}\ s^{-1}$ [25]) that is released by excited indole; (iii) the oxidation of indole by excited ferric iron; (iv) reduction of Fe^{3+} by excited indole. Under UV-A irradiation, mechanisms (ii) and (iv) should not be involved. We conducted a series of experiments to examine this.

The yield of HO• radical adducts from UV-B- and UV-A-induced photolysis of $FeOH^{2+}$ and $Fe(OH)_2^+$ was decreased in the presence of indole (Fig. 3a, b). Clearly, HO• scavenging contributes to indole-mediated Fe^{2+} accumulation. However, HO• scavenging activity of indole was significantly higher ($P < 0.05$) in iron-free HO•-generating system—UV-induced homolysis of H_2O_2 (Fig. 3c). This implies that a part of the reducing capacity of indole is 'invested' in other mechanisms. HO• shows very high reducing potential (E° = 2.31 V) [26], and easily reacts with indole and different

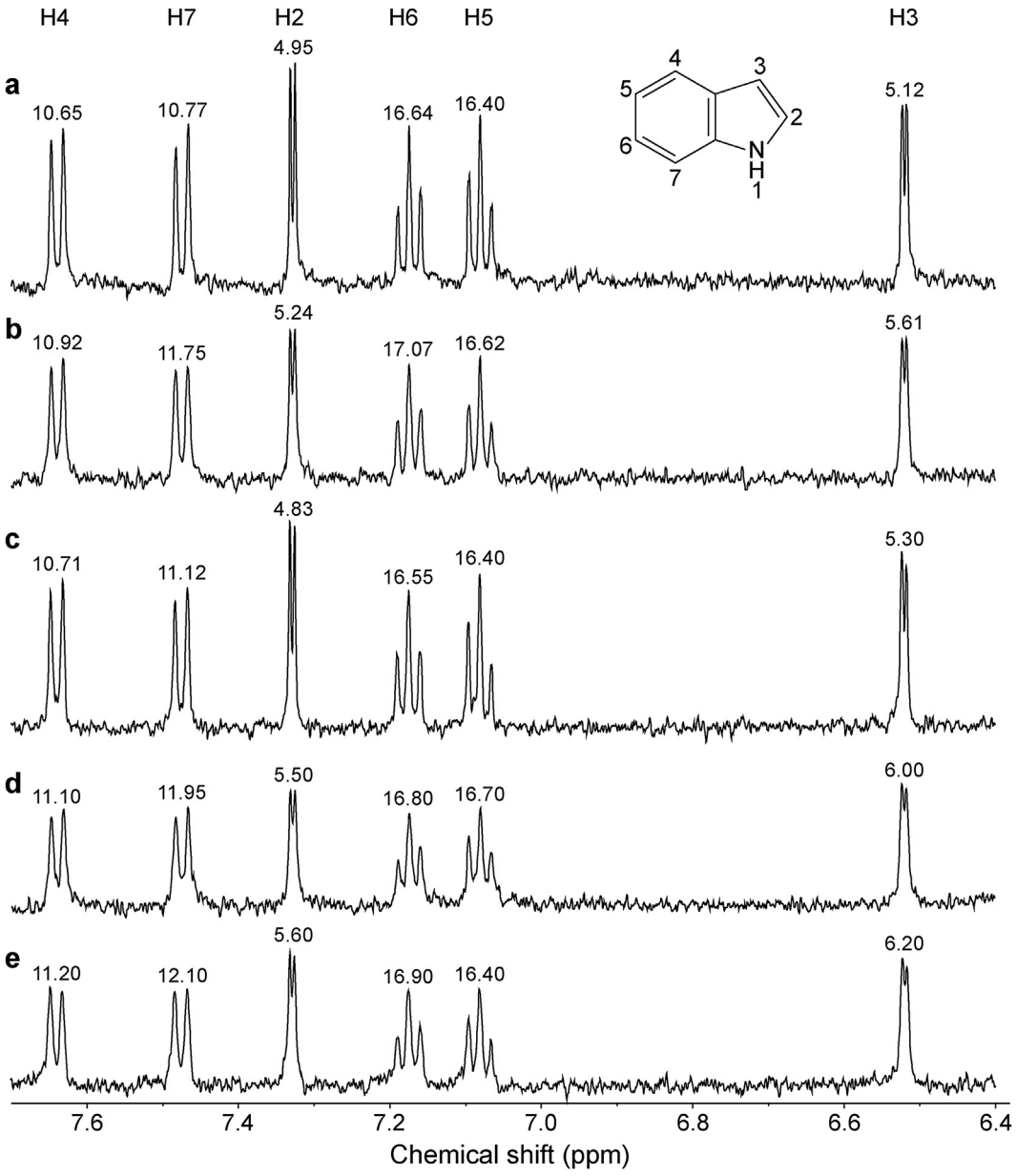

Fig. 4. Characteristic ^{1}H NMR spectra of indole in D_2O. (a) Indole (200 μM). (b) Indole (200 μM) + $FeCl_3$ (100 μM). (C) Indole (200 μM) + $FeCl_3$ (100 μM) + NaCl (1 mM). (d) Indole (200 μM) + $FeCl_2$ (100 μM). (e) Indole (200 μM) + $FeCl_2$ (100 μM) + NaCl (1 mM). Structure of indole and line widths at half height [Hz] for each multiplet are presented.

products of indole degradation [27]. For example, rate constants for reactions of HO• with indole (E° = 1.24 V) and with hydroxyindole (E° = 0.2 V) are $k = 3.2 \times 10^{10}$ and $k = 1.7 \times 10^{10}$ M^{-1} s^{-1}, respectively [25,26]. Higher anti-HO• activity under UV-B compared to UV-A can be attributed to a lower reducing potential of indole in excited, compared to a ground state (−3.08 V *vs.* 0.88 V for tryptophan [28]). It is important to note that photolysis of $Fe(OH)^{2+}$ and $Fe(OH)_2^+$ produce Fe^{2+} and HO• with 1:1 stoichiometry. Therefore, the overall effect on the amount of Fe^{3+} reduced to Fe^{2+} is the same, regardless of whether the indole and its derivatives react with HO• or donate electrons directly to Fe^{3+}.

The production of e_{aq^-} could not be detected using the settings from the previous set of experiments (indole, 200 μM; DEPMPO, 4 mM). Hence, a much higher concentration of indole (5 mM) was irradiated in H_2O and D_2O in the presence of high concentration of spin-trap DMPO (40 mM). DMPO/H and DMPO/D adducts were identified (Fig. 3d, e). The latter implies that there is no release of hydrogen atom from indole, since its protons are not prone to substitution. Instead, e_{aq}^- adducts were protonated by H^+ or D^+ from water. The presence of HO• (DO•) adducts might be related to the reaction of e_{aq}^- with O_2 that gives rise to superoxide radical anion. DMPO adduct of superoxide is known to rapidly convert to DMPO/OH [29]. DMPO/H(D) → DMPO/OH(OD) conversion is also plausible. The fact that EPR spin-trapping could detect e_{aq}^- only at very high indole and spin-trap concentrations implies that e_{aq}^- release by excited indole is not an efficient process. Oximetry was employed to further examine this. Electrons released by excited indole in the absence of iron can react with O_2 ($k = 1.9 \times 10^{10}$ M^{-1} s^{-1}) or H^+ ($k = 2.3 \times 10^{10}$ M^{-1} s^{-1}) [25]. In aerated water ([O_2] ≈ 300 μM) with pH 5, the reaction with O_2 clearly predominates, so the consumption of O_2 under such settings represents a measure of e_{aq}^- production. UV-B irradiation of 200 μM indole for 10 min resulted in 5 μM [O_2] decrease, whereas the irradiation of 1 mM led to a (proportional) 25 μM decrease (Fig. 3f). The presence of Fe^{3+} (100 μM) did not affect indole-related drop in [O_2] (not shown). This speaks in favor of a very weak production

of e_{aq}^- by the UV-B irradiated indole. It is noteworthy that the oxidation of Fe^{2+} with O_2 is very slow at pH 5 ($k \approx 10^{-3}\ M^{-1}\ s^{-1}$) [30]. As expected, UV-A did not cause any changes in [O_2] (not shown). In line with this, UV-A irradiation did not induce the formation of indole radical(s) in the iron-free system (Fig. 3g). On the other hand, the signal of indole-derived radical (probably $Ind^{\bullet+}$) with characteristic position at $g \approx 2$ was detected in UV-B-irradiated iron-free system (Fig. 3g). Both types of UV irradiation caused the production of indole-derived radical(s) in the presence of iron. Signal amplitude showed a linear increase with increasing $[Fe^{3+}]_i$ (Fig. 3h, i). This implies that the signal does not come only from the product of one-electron oxidation of indole, but also from a number of other radicals that emerge in reactions of indole and its derivatives with $HO^{\bullet}$ [27], or *via* oxidation of derivatives by Fe^{3+}. Pertinent to the latter, hydroxyindole might spontaneously reduce Fe^{3+}, taking into account the reducing potential of Fe^{3+}/Fe^{2+} pair ($E^{\circ} = 0.77$ V) [26]. These radicals do not have a well defined structure, *i.e.* unpaired electron can be located in different positions on the ring, resulting in a broad signal (line width ~10 G) with no hyperfine splitting (not observed even at modulation amplitude of 1 G). It is important to note that $Ind^{\bullet+}$ might undergo deprotonation to give rise to indolyl radical and H^+ [31], or it might react with water to give hydroxyindole radical and H^+ [32]. Either way, this should lead to a decrease in pH. A trend of pH decrease was observed during UV irradiation of indole in the presence of iron (Fig. S4).

3.3. Formation of iron–indole complex and its role in the reduction

Fe^{3+} and Fe^{2+} caused line broadening in indole ^1H NMR spectrum at positions C3, C2, and C7, implying that iron binds to indole (Fig. 4; Table S1). At these positions, indole ring shows the highest electron density and the largest HOMO π-orbital coefficients [33]. The coordination between Fe^{3+} and π-electronic system has been observed previously for indole-3-acetic acid and it involved C2 and C3 positions [34]. Fe^{3+} and high-spin Fe^{2+} are paramagnetic, whereas low-spin Fe^{2+} is diamagnetic. The fact that Fe^{3+} and Fe^{2+} provoked analogous changes in the spectral shape implies that high-spin Fe^{2+} binds to indole. This is in line with previous calculations that the complex of high-spin Fe^{2+} with benzene ring is more stable compared to low-spin Fe^{2+} [35]. Fe^{3+}-induced line broadening was annulled by Cl^- (Fig. 4c), which was not the case for Fe^{2+} (Fig. 4e). According to Pearson's HSAB principle, hard Lewis acids prefer hard bases as ligands. The same stands for borderline and soft acids/bases [36]. Fe^{3+} is a hard acid and prefers Cl^-, which is a hard base, compared to indole which is a borderline base [36,37]. Fe^{2+} is a borderline acid, so it prefers indole to Cl^-. Indole binding to Fe^{2+} might stabilize this form of iron in aqueous systems. Fig. 5a shows low-T EPR spectrum of Fe^{3+} in water. In the presence of indole, a broad signal in the lower field, which can be attributed to high-spin ($S = 5/2$) ferric iron in a low symmetry environment, showed increased amplitude (Fig. 5b). This further proves that indole forms complex with Fe^{3+}. An additional signal emerged in the higher field, which is related to low-spin ($S = 1/2$) Fe^{3+} complexes. The addition of Cl^- appears to affect Fe^{3+}–indole complex. A strong signal, probably from a tetrahedral complex emerged at $g = 4.3$, whereas the signal of low-spin Fe^{3+} showed decreased amplitude. It is important to note that chloride ions, at concentrations applied here, do not affect complexes of Fe^{3+} with OH^- ions [30,38]. Pertinent to this, changes observed here can be mainly attributed to the effects of Cl^- on iron–indole complex.

Iron-induced decomposition of indole under UV-B was partially prevented by Cl^- (Fig. 6a). On the other hand, Cl^- practically did not have any effect on the system exposed to UV-A (Fig. 6b). It is important to note that Cl^- did not affect UV effects on indole in the absence of iron. These results imply that Fe^{3+}–indole complex

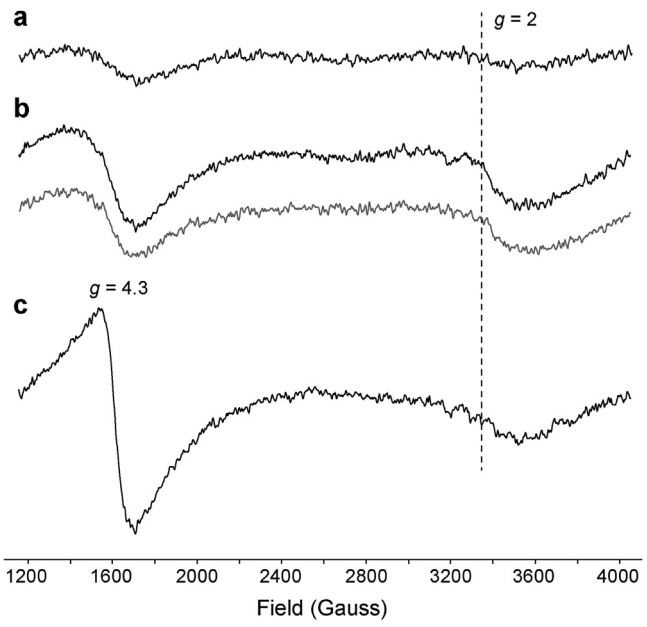

Fig. 5. 20 K EPR spectra of Fe^{3+}. (a) $FeCl_3$ (200 μM); (b) $FeCl_3$ (200 μM) + indole (1 mM). Gray line is the difference between (b) and (a); (c) $FeCl_3$ (200 μM) + indole (1 mM) + NaCl (1 mM).

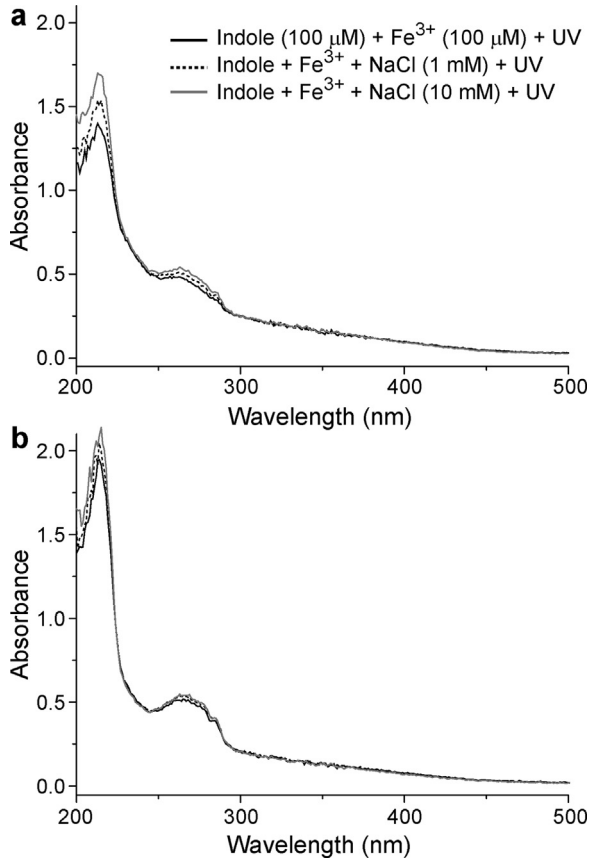

Fig. 6. Characteristic spectra illustrating the effects of NaCl on indole/Fe^{3+} system exposed to UV. (a) UV-B 3 J m^{-2} s^{-1}; (b) UV-A 3 J m^{-2} s^{-1}.

is important for reduction of Fe^{3+} by excited indole. Pertinent to this, it is known that indole-3-acetic acid and Fe^{3+} form a dimeric complex which is sensitive to Cl^-, and that the redox properties of indole ring are altered in this complex [39]. Finally, our findings are

in line with previous notions that chloride ions might slow down photo-Fenton degradation of some aromatic compounds [38,40].

4. Conclusion

Our results explain how indole promotes Fe^{3+} photo-reduction and Fe^{2+} accumulation in water systems. In total, oxidation/decomposition of one indole results in eight reduced ferric ions, irrespective of the type of UV irradiation (B or A). This process mainly runs indirectly, *via* scavenging of $HO^{\bullet}$ by indole and its derivatives, but directly as well, *via* oxidation of indole by excited ferric iron and reduction of Fe^{3+} by the excited indole. Of the two direct processes, the former appears to be more important, particularly if we take into account that the intensity of UV-A irradiance at sea level is considerably higher compared to UV-B. The reduction of iron by indole-released e_{aq}^- has only a minor role. Fe^{3+} and indole form weak low-symmetry complex which appears to be important for the reduction of Fe^{3+} by the excited indole. *Via* presented mechanisms, indole (and related aromatic compounds) might increase the pool of ferrous iron in aqueous systems that can further participate in various redox processes and that is available to living organisms. On the other hand, indole photo-degradation is facilitated in the presence of iron. UV, in combination with iron, might represent a useful tool in wastewater processing industry.

Acknowledgements

We are thankful to Dr. Nina Todorović at the Department of Chemistry, ICTM, University of Belgrade, for her kind help in obtaining NMR spectra. This work was supported by the Ministry of Education, Science and Technological Development of the Republic of Serbia, Grant numbers III43010, III41005, and 173014.

Appendix A. Supplementary data

Supplementary data associated with this article can be found, in the online version, at http://dx.doi.org/10.1016/j.apcatb.2015.12.018.

References

[1] W. Stumm, J.J. Morgan, Aquatic Chemistry; Chemical Equilibria and Rates in Natural Waters, third ed., John Wiley & Sons, New York, 1996.
[2] W. Feng, D. Nansheng, Chemosphere 41 (8) (2000) 1137–1147.
[3] E.W. Helbling, H. Zagarese, Comprehensive Series in Photochemical & Photobiological Sciences Volume 1: UV Effects in Aquatic Organisms and Ecosystems, Royal Society of Chemistry, Cambridge, 2003.
[4] R.G. Zepp, B.C. Faust, J. Hoigne, Environ. Sci. Technol. 26 (2) (1992) 313–319.
[5] P.G. Tratnyek, T.J. Grundl, S.B. Haderlein, Aquatic Redox Chemistry, American Chemical Society, Washington, 2011.
[6] B.M. Voelker, B. Sulzberger, Environ. Sci. Technol. 30 (4) (1996) 1106–1114.
[7] D. Naka, D. Kim, T.J. Strathmann, Environ. Sci. Technol. 40 (9) (2006) 3006–3012.
[8] J.B. Chen, B. Gu, R.A. Royer, W.D. Burgos, Sci. Total Environ. 307 (1–3) (2003) 167–178.
[9] S. Wuttke, S. El Naggar, T. Bluszcz, O. Schrems, Photochem. Photobiol. Sci. 6 (10) (2007) 1081–1088.
[10] G. Seckmeyer, D. Pissulla, M. Glandorf, D. Henriques, B. Johnsen, A. Webb, A.M. Siani, et al., Photochem. Photobiol. 84 (1) (2008) 172–179.
[11] W. Schüssler, L. Nitschke, Water Res. 33 (12) (1999) 2884–2887.
[12] O. Botalova, J. Schwarzbauer, T. Frauenrath, L. Dsikowitzky, Water Res. 43 (15) (2009) 3797–3812.
[13] J. Lin, J. Aoll, Y. Niclass, M.I. Velazco, L. Wünsche, J. Pika, C. Starkenmann, Environ. Sci. Technol. 47 (14) (2013) 7876–7882.
[14] J.R. Carney, F.C. Hagemeister, T.S. Zwier, J. Chem. Phys. 108 (9) (1998) 3379–3382.
[15] W.J. Tang, Q.H. Song, H.B. Wang, J.Y. Yu, Q.X. Guo, Org. Biomol. Chem. 4 (13) (2006) 2575–2580.
[16] H. Tian, Y. Guo, B. Pan, C. Gu, H. Li, S.A. Boyd, Environ. Sci. Technol. 49 (13) (2015) 7784–7792.
[17] J. Peon, G.C. Hess, J.L. Pecourt, T. Yuzawa, B. Kohler, J. Phys. Chem. A 103 (14) (1999) 2460–2466.
[18] C. Floxa, S. Ammarb, C. Ariasa, E. Brillasa, A.V. Vargas-Zavalac, R. Abdelhedib, Appl. Catal. B: Environ. 67 (1–2) (2011) 93–104.
[19] Y. Zhong, X. Liang, Z. He, W. Tan, J. Zhu, P. Yuan, R. Zhu, et al., Appl. Catal. B: Environ. 150–151 (2014) 612–618.
[20] K. Makino, M.M. Mossoba, P. Riesz, J. Phys. Chem. 87 (1983) 1369–1377.
[21] M.J. Davies, S. Fu, R.T. Dean, Biochem. J. 305 (2) (1995) 643–649.
[22] A. Stefánsson, Environ. Sci. Technol. 41 (17) (2007) 6117–6123.
[23] V. Nadtochenko, J. Kiwi, Inorg. Chem. 37 (20) (1998) 5233–5238.
[24] R.J. Sundberg, Indoles, Academic Press Limited, London, 1996.
[25] G.V. Buxton, C.L. Greenstock, W.P. Helman, B. Ross, J. Phys. Chem. Ref. Data 17 (2) (1988) 513–866.
[26] P. Wardman, J. Phys. Chem. Ref. Data 18 (4) (1989) 1637–1755.
[27] B. Iddon, G.O. Phillips, K.E. Robbins, J.V. Davies, J. Chem. Soc. B (1971) 1887–1892.
[28] J.H. Zhou, X.H. Wu, C. Yang, X.T. Gu, L. Zhou, K.X. Song, Y.Y. Feng, J. Shen, Spectroscopy 21 (4) (2007) 235–243.
[29] I. Spasojević, Crit. Rev. Clin. Lab. Sci. 48 (3) (2011) 114–142.
[30] J. Kiwi, A. Lopez, V. Nadtochenko, Environ. Sci. Technol. 34 (11) (2000) 2162–2168.
[31] L. Candeias, L. Folkes, M. Dennis, K. Patel, S. Everett, M. Stratford, P. Wardman, J. Phys. Chem. 98 (1994) 10131–10137.
[32] F. Rollet, C. Richard, J.F. Pilichowski, B. Aboab, Org. Biomol. Chem. 2 (15) (2004) 2253–2261.
[33] A. Chrostowska, S. Xu, A. Mazière, K. Boknevitz, B. Li, E.R. Abbey, A. Dargelos, et al., J. Am. Chem. Soc. 136 (33) (2014) 11813–11820.
[34] A.A. Kamnev, A.G. Shchelochkov, P.A. Tarantilis, M.G. Polissiou, Y.D. Perfiliev, Monatsh. Chem. 132 (6) (2001) 675–681.
[35] S. Kolakkandy, S. Pratihar, A.J. Aquino, H. Wang, W.L. Hase, J. Phys. Chem. A 118 (40) (2014) 9500–9511.
[36] K.L. Haas, K.J. Franz, Chem. Rev. 109 (10) (2009) 4921–4960.
[37] A. Chatterjee, T. Ebina, T. Iwasaki, J. Phys. Chem. A 105 (47) (2001) 10694–10701.
[38] A.J. Machulek, J.E. Moraes, C. Vautier-Giongo, C.A. Silverio, L.C. Friedrich, C.A. Nascimento, M.C. Gonzalez, et al., Environ. Sci. Technol. 41 (24) (2007) 8459–8463.
[39] K. Kovács, V.K. Sharma, A.A. Kamnev, E. Kuzmann, Z. Homonnay, A. Vértes, Struct. Chem. 19 (1) (2008) 109–114.
[40] J.E. Moraes, F.H. Quina, C.A. Nascimento, D.N. Silva, O. Chiavone-Filho, Environ. Sci. Technol. 38 (4) (2004) 1183–1187.